Self-Decoupled Multiantennas With Coupling Modes Identification and Suppression

Hui Li, *Senior Member, IEEE*, Yang Nan, Jia-Wen Xu, Qiang Chen, *Senior Member, IEEE*, and Tian-Xi Feng, *Member, IEEE*

***Abstract*—In this letter, a self-decoupling method is proposed for multi antenna systems based on the identification and suppression of coupling modes. Coupling modes are first identified by characteristic mode analysis, with the coupled power due to each mode quantitatively monitored for the first time. Together with the modal weighting coefficients, the coupling modes to be suppressed are determined. Antennas are then adjusted to break the high-coupling modes without affecting the radiating modes, leading to enhanced isolations. An example involving two identical side-by-side metasurface-based patch antennas with extremely close proximity ($0.014\lambda_0$) is given. By etching slits at the proper locations of the antennas, the coupling modes have been effectively suppressed without compromising the primary radiation. As a result, the isolations between the antennas are significantly improved by more than 15 dB without additional decoupling structures. The patterns are restored as well. Measurements have been conducted on the antenna systems, showing the feasibility of the self-decoupling method.**

***Index Terms*—Characteristic mode (CM) analysis, multiantenna system, mutual coupling, self-decoupling.**

I. Introduction

THE proliferation of antennas has witnessed a substantial surge in both terminal devices and base stations in recent years [1], [2]. As a result, mutual coupling greatly deteriorates wireless system performance. Significant efforts have been dedicated to mitigating the mutual coupling between antennas. In general, antenna decoupling techniques can be classified as coupling blocking, coupling cancellation, and self-decoupling methods.

The coupling blocking technique entails the introduction of isolation structures or materials between antennas to obstruct the mutual coupling path. Various structures, such as split-ring resonators (SRRs) [3] and electromagnetic bandgap (EBG) structures [4] can be inserted between antennas to directly block the coupling paths. In [5], a thin magnetic metamaterial is embedded in the dielectric substrate to cut off the propagation of electromagnetic waves in the dielectric layer. Alternatively, the coupling paths can be blocked by transferring the power to the nearby elements [6], [7], [8]. However, the coupling blocking method typically necessitates additional structures.

The coupling cancelation technique achieves decoupling by establishing additional coupling paths that have opposite phases but similar amplitude to the original coupling path. Prevalent approaches include the neutralization lines (NL) [9] and the parasitic elements [10], [11], [12]. However, adding more decoupling structures complicates multiantenna systems and reduces reliability.

Recently, self-decoupling technique that leverages the inherent characteristics of the antennas to enhance isolations has attracted increasing attention. In [13], [14], and [15], the adjacent antenna is strategically arranged in the weak-field region of the excited antenna, leading to higher isolations. However, the placement of antennas is constrained by the zero-field regions. A decoupling method based on common mode and differential mode is proposed in [16]. In addition to the approaches above, characteristic mode (CM) theory has also been employed. The work in [17] employs higher-order characteristic modes by incorporating ring structures to disperse coupled power and enhance port isolation.

This letter takes a distinct approach, where the inherent coupling ability of each mode is quantitatively investigated, making the coupling mechanism clear. High-coupling modes and low-coupling modes are identified first by using characteristic far-field patterns as the excitations. Afterward, by comparing the total current distributions of the antenna and the characteristic currents of the high-coupling modes, antenna structures are slightly modified to suppress the high-coupling modes while maintaining the original radiation, leading to higher isolations. The contributions of the letter lie in the following:

1) the coupling ability of each characteristic mode is quantified for the first time, providing insight into the mechanism of mutual coupling;
2) the proposed method is not only applied to a specific structure, but can generally be applied to antennas with multiple modes; and
3) extremely small mutual distance between the antennas can be achieved without additional decoupling structures or specific antenna arrangement.

II. Self-Decoupling With Highly Coupled CMs

A. Theory

To investigate the coupling quantitively from the perspective of CM theory, some basic metrics of CM are reviewed first. The CM of perfect electric conductor (PEC) can be obtained by

Manuscript received 20 May 2024; revised 24 June 2024; accepted 9 July 2024. Date of publication 18 July 2024; date of current version 8 October 2024. This work was supported in part by the National Natural Science Foundation of China under Grant 61971087 and Grant 62371089. *(Corresponding author: Tian-Xi Feng.)*

Hui Li, Yang Nan, Jia-Wen Xu, and Tian-Xi Feng are with the School of Information and Communication Engineering, Dalian University of Technology, Dalian 116024, China (e-mail: fengtianxi@dlut.edu.cn).

Qiang Chen is with the Research Institute of Electrical Communication, Tohoku University, Sendai 980-8577, Japan.

Digital Object Identifier 10.1109/LAWP.2024.3430372

solving the generalized eigenvalue equation

$$\mathbf{X}\mathbf{J}_n = \lambda_n \mathbf{R}\mathbf{J}_n \tag{1}$$

where λ_n represents the eigenvalues associated with the characteristic current $\mathbf{J}_n$, $\mathbf{R}$ and $\mathbf{X}$ denote the real and imaginary parts of the impedance matrix [18]. As an alternative way to represent the eigenvalues, modal significance (MS) is defined as

$$\mathrm{MS}_n = \left| \frac{1}{1 + j\lambda_n} \right| \tag{2}$$

which maps the eigenvalues to (0, 1]. When MS approaches 1, the mode is easily excited. In contrast, when MS is close to 0, it is difficult to excite the mode.

According to CM theory, the total currents on the antenna surface can be regarded as a linear combination of a series of characteristic currents

$$\mathbf{J} = \sum_{n=1}^{N} \alpha_n \mathbf{J}_n \tag{3}$$

where α_n represents the modal weighting coefficient (MWC) of the *n*th characteristic mode, indicating the contribution of the mode in generating the target current.

For a dual-antenna system, one antenna is designated as the transmitting (Tx) antenna, while the other serves as the receiving (Rx) antenna. According to the equivalent circuit of the Rx antenna, the power flowing into the load of the RX antenna can be expressed as [19]

$$P = \frac{1}{2} \frac{g_L}{|Y_a + Y_L|^2} |I_r|^2 \tag{4}$$

where Y_a is the admittance of the antenna, $Y_L$and g_L are the admittance and conductance of the load, respectively. I_r is the current at the port. Normally, $g_L = Y_L = \frac{1}{50}S$.

Antenna decoupling aims at reducing the power flown to the Rx antenna. Therefore, the coupled current at the port should be minimized. Each normalized characteristic current of the Tx antenna $\mathbf{J}_{\mathrm{n,t}}$ induces certain currents $I_{n,r}$ at the port of the Rx antenna. Hence, the total current at the Rx antenna is expressed as

$$I_r = \sum_{n=1}^{N} \frac{\langle \boldsymbol{J}_n, \boldsymbol{E}^i \rangle}{1 + j\lambda_n} I_{n,r} = \sum_{n=1}^{N} \alpha_n I_{n,r}. \tag{5}$$

In (5), $\alpha_n$is the MWC of the *n*th mode of the Tx antenna. The total coupled current is influenced by two key factors. On one hand, it depends on the coupling capability of the modal currents, as different modal currents of the Tx antenna result in distinct coupled currents. On the other hand, it hinges on the excitation level of the *n*th mode of the Tx antenna, i.e., α_n. By changing the feeding structure, the incident electric field $\boldsymbol{E}^i$ becomes different. In this letter, the feeding structure is fixed for fair comparisons between antennas before and after decoupling. This way, the incident electric field $\boldsymbol{E}^i$ and the mutual distance between the feedings are unchanged. The decoupling is only owing to the mode suppression.

The primary objective of this letter is to pinpoint high-coupling modes that lead to large $I_{n,r}$. Through minor adjustments to the antenna structure, the excitation of these modes can be effectively suppressed, leading to reduced coupled power and enhanced port isolation.

B. Design Procedures

The workflow of the self-decoupling method is presented in Fig. 1. The design procedures are outlined as follows.

1) Characteristic mode analysis is conducted on antenna 1 within the target frequency band to obtain the MWC for each mode. The modes with high MWCs are highly excited modes.
2) The characteristic far-field of each mode is normalized and imported into FEKO, which replaces antenna 1 as the source to excite antenna 2. The coupled current generated at port 2 is monitored for each mode. The coupled power is then calculated according to (4), which indicates the coupling capability of the mode.
3) The modes with high MWC and high coupled power are determined as the high-coupling characteristic modes.
4) The total currents of antenna 1 are compared with the characteristic currents of each high-coupling mode. If the currents are similar even in local areas, the mode is maintained as the radiating mode. If the currents are different in some local areas, modifications can be made at those local areas of antenna 1 to suppress the coupling mode without affecting the total radiation. Consequently, the isolations between antennas can be improved.
5) If the two antennas are identical, the same modifications are made on antenna 2. Otherwise, the same procedures from (1)–(4) are carried out again for antenna 2.

Since the proposed method is based on mode suppression, it is suitable for antennas with multiple modes, including some simple decoupling cases, i.e., two side-by-side patch antennas.

III. Self-Decoupled Metasurface Antenna Array

In this section, a practical MIMO antenna system based on metasurface (MTS) is presented to validate the effectiveness of the proposed self-decoupling method. MTS antennas are employed since they provide multiple modes, clear current distributions and high gain. The dimensions of the MTS antenna are similar to other MTS antennas in the literature [20], [21].

A. Antenna Configuration

The original configurations of the MTS antennas for the 5G Wi-Fi frequency band are illustrated in Fig. 2. Each antenna consists of three metallic layers: the MTS layer, the ground plane and the feeding layer with the microstrip line. Each MTS antenna is composed of 3 × 3 square patch units. The two MTS-based patch antennas are placed side by side, with a very close distance of 0.8 mm ($0.014\lambda_0$), which is the same as that between the MTS units. The MTS antennas are coupled and fed by the slots on the ground plane. Dielectric of F4BM350 is employed, with a relative permittivity of 3.5 and a loss tangent of 0.001.

The exceptionally small distance between the antennas results in high mutual coupling, which alters the original performance of the MTS patch antennas, including both the reflection properties and the radiation pattern. The reflection coefficients of the isolated MTS antenna are compared with those of the MTS antenna in the MIMO system in Fig. 3(a). The mutual couplings of around −10 dB are observed. Besides, an additional resonance is induced at 5.1 GHz due to mutual coupling.

For comparison, the radiation patterns of the isolated MTS antenna and the MTS antenna in the MIMO system are displayed in Fig. 3(b). Since the two antennas are symmetrically located,

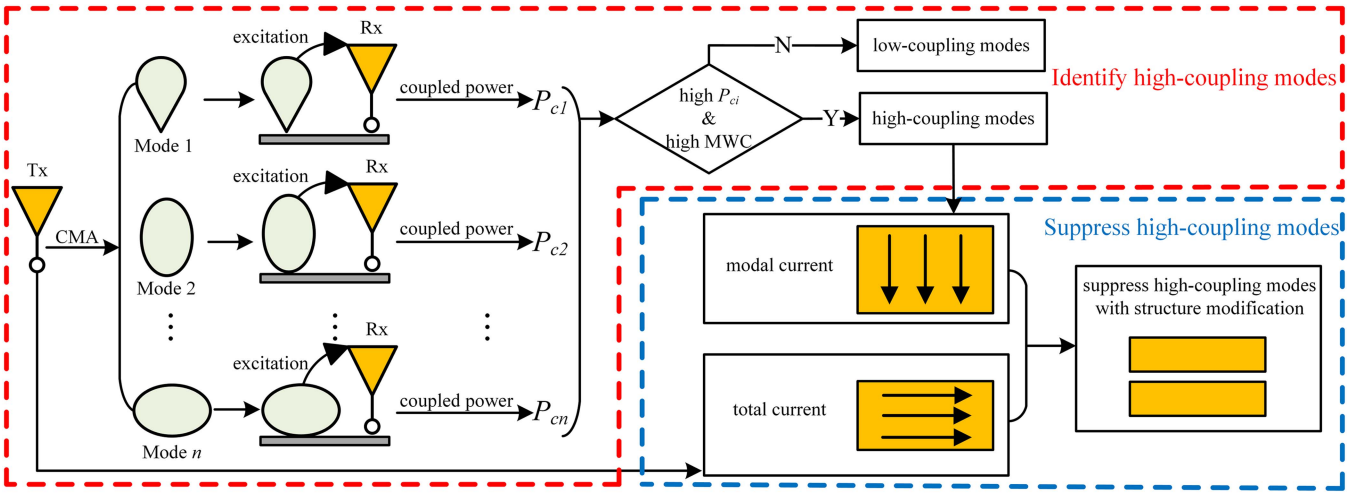

Fig. 1. Flowchart of the proposed self-decoupling method. Two main steps include the high-coupling modes identification and the high-coupling modes suppression.

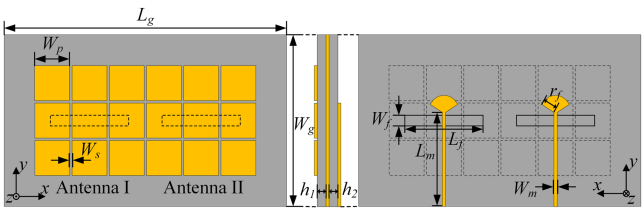

Fig. 2. Configurations of the MTS antenna array. ($L_g = 92.6$, $L_f = 25$, $L_m = 28.9$, $W_g = 56.3$, $W_f = 1.5$, $W_m = 1.1$, $W_p = 11.3$, $W_s = 0.8$, $h_1 = 3$, $h_2 = 0.5$, $g = 0.5$, $r_f = 5.4$. Unit: mm.)

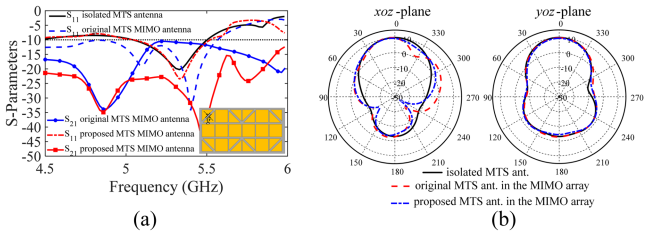

Fig. 3. (a) *S*-parameters of the isolated MTS antenna and the MTS antenna in the MIMO array. (b) Far-field patterns at 5.3 GHz for the isolated MTS antenna, the original MTS antenna in the MIMO array, and the proposed MTS antenna in the MIMO array.

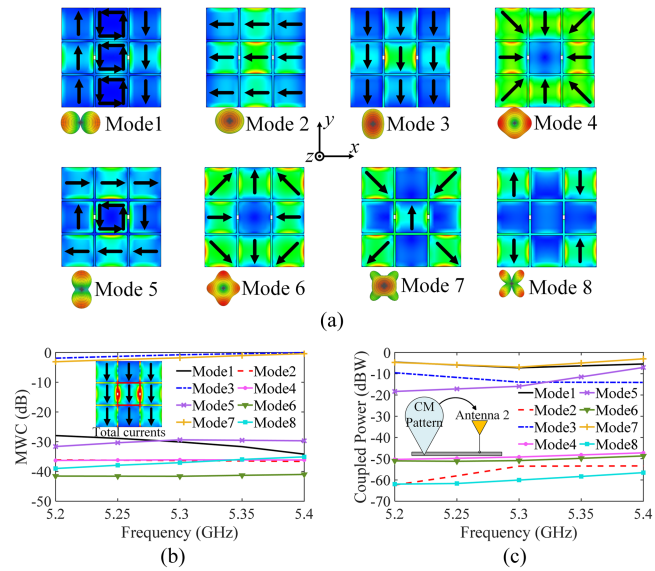

Fig. 4. (a) Modal currents and modal fields of the MTS antenna. (b) MWCs of the first eight modes of the MTS antenna. (c) Coupled power of each mode to the Rx MTS antenna.

only the radiation pattern of antenna 1 is given at its resonance. It reveals that the radiation pattern of the MTS antenna within the array experiences significant distortion compared with that of the isolated antenna.

B. Self-Decoupled MTS Antennas

In order to reduce the mutual coupling and restore the radiation pattern of the isolated antenna, the self-decoupling method in Section II is applied.

CM analysis is performed on the MTS antenna at the frequency range of 5.2 GHz to 5.4 GHz using the commercial simulation software FEKO. The characteristic far-field patterns and characteristic currents of the first eight significant modes of the MTS antenna are shown in Fig. 4(a). The design process is given as follows.

1) First, the MWCs are calculated for the eight modes, as shown in Fig. 4(b). It can be observed that modes 3 and 7 are significantly excited.
2) The normalized characteristic pattern of each mode is employed in FEKO to replace antenna 1 and utilized as the excitation for antenna 2, as indicated in the inset of Fig. 4(c). The coupled current is then monitored at the port of antenna 2, with which the coupled power is calculated, as presented in Fig. 4(c). Modes 1, 3, 5, and 7 exhibit high coupling to antenna 2, whereas the remaining modes show coupled power of approximately 30 dB lower.
3) Together with the MWC curves, it is derived that modes 3 and 7 are high-coupling modes.
4) The total current distributions of the antenna at 5.3 GHz are depicted in the inset of Fig. 4(b). It is observed that the current distributions associated with mode 3 align with the

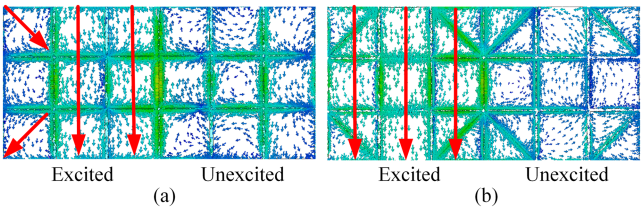

Fig. 5. Current distributions of the MTS antennas at 5.3 GHz: (a) initial antennas and (b) self-decoupled antennas.

antenna's total currents. Thus, mode 3 should be preserved as the radiating mode. In contrast, the currents of mode 7 are different from the total currents, especially at the four corner patches. Hence, mode 7 is identified as the high-coupling mode to be suppressed.

5) Slots with a width of 0.5 mm along the diagonals of the patches at the four corners are introduced to disrupt the current distributions of mode 7. Since the two antennas are identical, the same modifications are applied to antenna 2.

The *S*-parameters of the proposed antennas are compared with the original ones in Fig. 3(a), with the configuration given in the inset. The operating frequency band covers 5.07 GHz to 5.55 GHz, which remains consistent with that of the isolated MTS antenna. The additional resonance caused by mutual coupling has been removed. The isolations between the antennas are above 20 dB throughout the entire operating band, with the best isolation reaching 45 dB close to the resonance.

Fig. 5 compares the currents on the antennas before and after decoupling when antenna 1 is excited. Before decoupling, the currents of the excited antenna concentrate on the middle and right columns of patches, and diagonal currents are observed on the patches on the left column due to the existence of mode 7. Besides, strong currents are observed along the edges of the unexcited antenna. With the modified structure, vertical currents are evenly distributed on the excited antenna, attributed to the suppression of mode 7. At the same time, the currents generated on the unexcited antenna are significantly reduced. The radiation patterns of the MTS antennas after decoupling are given in Fig. 3(b). After decoupling, the radiation pattern has been restored to match that of the isolated antenna at 5.3 GHz. In other words, pattern distortion has been eliminated despite their close proximity.

C. Experiment of the MTS-Based MIMO Antennas

To validate the simulation results, a prototype of the self-decoupled MTS-based MIMO antenna system was fabricated, with the prototype given in Fig. 6(a). Considering practical feeding issues, two rectangular patches, which were connected to the ground plane through vias, were printed on the feeding layer. SMA connectors were used to feed the antenna through the microstrip line and the rectangular patches.

The reflection coefficients of the proposed self-decoupled antennas were measured using Agilent E5071C vector network analyzer, with the results shown and compared with the simulated ones in Fig. 6(b). The measured results agreed well with the simulated ones, with small discrepancies attributed to the cable and the soldering influence. The measured port isolations were above 20 dB over the entire operating band.

Due to the symmetric configuration, the radiation patterns of only antenna 1 were measured in the anechoic chamber, with the measurement setup given in Fig. 6(a). The simulated and measured radiation patterns were compared in Fig. 6(c), which agreed well with each other as well.

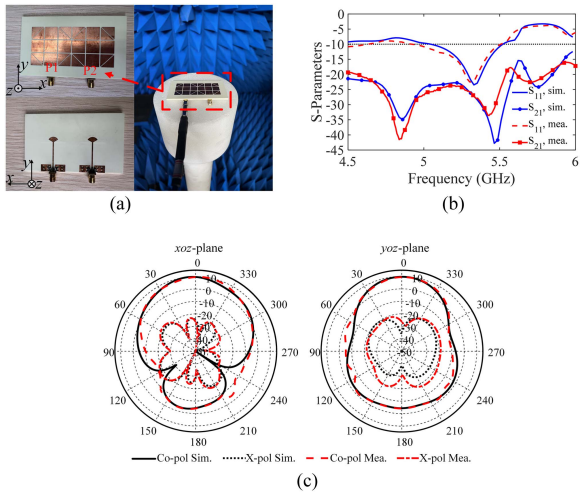

Fig. 6. (a) Photographs of the fabricated prototype and the measurement setup. (b) Simulated and measured *S*-parameters of the self-decoupled MTS antenna array. (c) Simulated and measured radiation patterns at 5.3 GHz.

TABLE I
COMPARISON WITH OTHER DECOUPLING METHODS

Ref.	Method	EES (λ_o)	bandwidth	Isolation (dB)
[3]	SRR	0.08	11.1%	From 17 to 25
[4]	EBG	0.22	2.5%	From 15 to 30
[9]	NL	0.04	24%	From 10 to 20
[15]	Self-decoupled	0.13	6.7%	From 18 to 30
Proposed	**Self-decoupled**	**0.014**	**9%**	**From 10 to 20**

(λ_o is the free-space wavelength at the center frequency; EES: edge-to-edge spacing)

D. Performance Comparison

Table I compares the state-of-the-art decoupling structures in terms of antenna spacing and isolation levels. The isolations between antennas are normally improved by around 10 dB using the decoupling techniques. Among those antennas, the mutual distance between the proposed antennas is extremely small, especially compared with other self-decoupling methods. Besides, the bandwidth of the antennas is relatively large after decoupling. The proposed method provides a step-by-step approach to decoupling the antenna without additional structures.

IV. CONCLUSION

In this letter, a self-decoupling technique that quantitatively describes the coupling ability of each mode has been proposed. By analyzing the MWC and the coupled power at the Rx antenna, high-coupling modes are first identified. To disturb the high-coupling modes while preserving the original radiation, antenna structures are adjusted. Substantial isolation enhancement has been achieved, as demonstrated by the side-by-side MTS array. The proposed method has also been successfully applied to antenna systems with different antennas, and it is generally suitable for antennas with multiple modes.

REFERENCES

[1] P. Sharma, R. N. Tiwari, P. Singh, P. Kumar, and B. K. Kanaujia, "MIMO antennas: Design approaches, techniques and applications," *Sensors*, no. 20, pp. 7813–7815, Oct. 2022.

[2] M. A. Jensen and J. W. Wallace, "A review of antennas and propagation for MIMO wireless communications," *IEEE Trans. Antennas Propag.*, vol. 52, no. 11, pp. 2810–2824, Nov. 2004.

[3] M. Li, X. Chen, A. Zhang, W. Fan, and A. A. Kishk, "Split-ring resonator-loaded baffles for decoupling of dual-polarized base station array," *IEEE Antennas Wireless Propag. Lett.*, vol. 19, no. 10, pp. 1828–1832, Oct. 2020.

[4] X. Yang, Y. Liu, Y. Xu, and S. Gong, "Isolation enhancement in patch antenna array with fractal UC-EBG structure and cross slot," *IEEE Antennas Wireless Propag. Lett.*, vol. 16, pp. 2175–2178, 2017.

[5] H. Zhang, J. Wang, X. Fu, Z. Chu, T. Liu, and S. Qu, "Decoupling patch antenna array using magnetic metamaterials," in *IEEE 4th Int. Conf. Electron. Inf. Commun. Technol.*, 2021, pp. 342–344.

[6] F. Liu, J. Guo, L. Zhao, G. Huang, Y. Li, and Y. Yin, "Dual-band metasurface-based decoupling method for two closely packed dual-band antennas," *IEEE Trans. Antennas Propag.*, vol. 68, no. 1, pp. 552–557, Jan. 2020.

[7] F. Liu, J. Guo, L. Zhao, X. Shen, and Y. Yin, "A meta-surface decoupling method for two linear polarized antenna array in sub-6 GHz base station applications," *IEEE Access*, vol. 7, pp. 2759–2768, 2019.

[8] J. Guo, F. Liu, L. Zhao, Y. Yin, G. Huang, and Y. Li, "Meta-surface antenna array decoupling designs for two linear polarized antennas coupled in H-plane and E-plane," *IEEE Access*, vol. 7, pp. 100442–100452, 2019.

[9] C.-D. Xue, X.-Y. Zhang, Y. F. Cao, Z. Hou, and C. F. Ding, "MIMO antenna using hybrid electric and magnetic coupling for isolation enhancement," *IEEE Trans. Antennas Propag.*, vol. 65, no. 10, pp. 5162–5170, Oct. 2017.

[10] W. Yang, L. Chen, S. Pan, W. Che, and Q. Xue, "Novel decoupling method based on coupling energy cancellation and its application in 5G dual-polarized high-isolation antenna array," *IEEE Trans. Antennas Propag.*, vol. 70, no. 4, pp. 2686–2697, Apr. 2022.

[11] C. Wei, Z. Y. Zhang, and K. L. Wu, "Phase compensation for decoupling of large-scale staggered dual-polarized dipole array antennas," *IEEE Trans. Antennas Propag.*, vol. 68, no. 4, pp. 2822–2831, Apr. 2020.

[12] M. Li and S. Cheung, "Isolation enhancement for MIMO dielectric resonator antennas using dielectric superstrate," *IEEE Trans. Antennas Propag.*, vol. 69, no. 7, pp. 4154–4159, Jul. 2021.

[13] H. Lin, Q. Chen, Y. Ji, X. Yang, J. Wang, and L. Ge, "Weak-field-based self-decoupling patch antennas," *IEEE Trans. Antennas Propag.*, vol. 68, no. 6, pp. 4208–4217, Jun. 2020.

[14] P. Kumari and S. Das, "A MIMO antenna system using self-decoupled EM-SIW dual-beam antenna elements," *IEEE Access*, vol. 10, pp. 1339–1345, 2022.

[15] Q. Lai, Y. Pan, and S. Zheng, "A self-decoupling method for MIMO antenna array using characteristic mode of ground plane," *IEEE Trans. Antennas Propag.*, vol. 71, no. 3, pp. 2126–2135, Mar. 2023.

[16] L. Sun, Y. Li, Z. Zhang, and H. Wang, "Antenna decoupling by common and differential modes cancellation," *IEEE Trans. Antennas Propag.*, vol. 69, no. 2, pp. 672–682, Feb. 2021.

[17] D. Zhang, Y. Chen, and S. Yang, "A self-decoupling method for antenna arrays using high-order characteristic modes," *IEEE Trans. Antennas Propag.*, vol. 70, no. 4, pp. 2760–2769, Apr. 2022.

[18] Y. Chen and C. Wang, *Characteristic Modes: Theory and Applications in Antenna Engineering*. Hoboken, NJ, USA: Wiley, 2015.

[19] J. Van Bladel, "On the equivalent circuit of a receiving antenna," *IEEE Antennas Propag. Mag.*, vol. 44, no. 1, pp. 164–165, Feb. 2002.

[20] F. H. Lin and Z. N. Chen, "Low-profile wideband metasurface antennas using characteristic mode analysis," *IEEE Trans. Antennas Propag.*, vol. 65, no. 4, pp. 1706–1713, Apr. 2017.

[21] X. Yang, Y. Liu, and S. X. Gong, "Design of a wideband omnidirectional antenna with characteristic mode analysis," *IEEE Antennas Wireless Propag. Lett.*, vol. 17, no. 6, pp. 993–997, Jun. 2018.